J. Fluid Mech. (2000), *vol.* 417, *pp.* 183–209. Printed in the United Kingdom

© 2000 Cambridge University Press

Reynolds-averaged equations for free-surface flows with application to high-Froude-number jet spreading

By WEN-LING HONG[1] AND DAVID T. WALKER[1,2]

[1]Department of Naval Architecture and Marine Engineering, University of Michigan, Ann Arbor, MI 48109-2145, USA

[2]Earth Sciences Group, Veridian ERIM International, Inc., PO Box 134008, Ann Arbor, MI 48113-4008, USA

(Received 24 August 1999 and in revised form 10 March 2000)

The goals of this study were to develop a set of Reynolds-averaged governing equations for turbulent free-surface flow, and to use the resulting equations to determine the origin of the surface current in high-Froude-number jet flows. To develop the Reynolds-averaged equations, free-surface turbulent flow is treated as a two-fluid flow separated by an interface. It is shown that the general Navier–Stokes equations written for variable property flow embody the field equations applicable to each fluid, as well as the boundary conditions for the interface and, therefore, can be applied across the entire fluid domain, including the interface. With this as a starting point, a formulation of the Reynolds-averaged governing equations for turbulent free-surface flows can be developed rigorously. The resulting Reynolds-averaged equations are written in terms of density-weighted averages, their derivatives, and the probability density function for the free-surface position. These equations are similar to the conventional Reynolds-averaged equations, but include additional terms which represent the average effect of the forces acting instantaneously on the free surface, forces normally associated with the boundary conditions. These averaged equations are applied to the interaction of a turbulent jet with the free surface in order to establish, for arbitrary-Froude-number flows, the origin of the surface current, the large outward velocity which occurs in a thin layer adjacent to the surface. It is shown via an order-of-magnitude analysis that the outward acceleration associated with the surface current results from a combination of the Reynolds-stress anisotropy and the free-surface fluctuations. For low Froude number, the surface current is mainly driven by the Reynolds stress anisotropy, consistent with the results of Walker (1997); when the Froude number is large, the Reynolds-stress anisotropy is smaller and the free-surface fluctuations make a significant contribution.

1. Introduction

Engineering predictions for turbulent flow near a free surface are of interest in applications ranging from ship hydrodynamics to manufacturing processes. The nonlinear nature of free-surface boundary conditions, along with the nonlinearity of the underlying Navier–Stokes equations, make this problem analytically intractable, and computationally challenging as well. The presence of a moving boundary presents some difficulty even for simple laminar flows, because the location of the boundary

is part of the solution of the fluid-flow problem. For turbulent flows, where many of the details must be captured by modelling, this is even more difficult. Because of these problems, some of the phenomena observed in free-surface flows remain unexplained. The goals of this study were to develop an analytical framework within which turbulent free-surface flow can be treated, and use that framework to address one of the outstanding gaps in our understanding of these flows.

The first objective of the study described herein was the development of an appropriate form of the Reynolds-averaged equations for turbulent free-surface flow. In many real-world flows, the free surface moves in an unsteady manner in response to the turbulent velocity and pressure fluctuations both above and below it. In most cases, engineering predictions of these flows make use of the Reynolds-averaged Navier–Stokes (RANS) equations. Because of the unsteady motion of the free surface, the free-surface boundary ceases to be distinct in the context of these averaged equations, and is 'smeared' over a region in space. The forces acting instantaneously on the boundary are effectively distributed over this region in a manner determined by the nature of both the free-surface fluctuations and the averaging process. The approaches previously developed for turbulent flow near a free surface are for flows with a steady free surface, either flat or with steady-state surface deformations (see e.g. Tahara & Stern 1996; Naot & Rodi 1982). In these approaches, the averaged form of the free-surface boundary conditions is applied at the steady free-surface location. In these approaches, the generation of unsteady surface disturbances by the subsurface turbulence has been ignored. If the surface is moving owing to the presence of turbulence-generated disturbances, this approach is questionable, at best, since application of the instantaneous free-surface boundary conditions at the instantaneous free surface will not, under a time average, reduce to the time-averaged free-surface boundary conditions applied at the average position of the free surface.

A candidate form for Reynolds-averaged equations appropriate for free-surface flows will be developed below. It will be shown that the general form of the Navier–Stokes equations, written for non-constant-property, incompressible, Newtonian flow can be applied globally to a two-fluid-flow problem, i.e. the equations can be applied across both fluids and the interface between them, in the manner of the level-set method of Chang *et al.* (1996). Since these equations apply to both fluids plus the interface, they can be time-averaged at a point in space to develop the Reynolds-averaged equations. The resulting equations are most conveniently written in terms of density-weighted averages, which reduce to simple time averages at positions removed from the fluctuating free surface. These equations are identical to the RANS equations except for some additional terms which appear on the right-hand side of the momentum equations which represent the effects of the fluctuating density (caused by the free-surface fluctuations) and the pressure forces acting instantaneously on the surface. The latter appear as effective body forces in the mean equations of motion; where in space they appear depends on the probability density function (p.d.f.) for free-surface position.

The second objective of the study was to attempt to resolve a paradox arising from the results presented by Walker (1997), involving the origin of the surface current in turbulent free-surface flows. In that study, which was limited to low Froude numbers (Froude number and Reynolds number are defined in terms of jet-exit velocity and jet diameter), the surface current – the large transverse velocity parallel to the free surface which develops when a turbulent flow such as a jet or wake interacts with a free surface – was attributed to the near-surface turbulent-stress anisotropy. As will be shown in the next section, high-Froude-number flows exhibit

a similar (or even larger) surface current, but have much lower levels of anisotropy. Application of an order-of-magnitude analysis similar to that used by Walker (1997) to the above-described Reynolds-averaged equations shows that for arbitrary-Froude-number flows, the surface current is caused by a combination of anisotropy and the net effect of the pressure forces acting on the fluctuating free surface. In low-Froude-number flows, the anisotropy dominates, whereas in high-Froude-number flows, the fluctuating surface forces make a significant contribution.

In § 2 below, some experimental data is presented for turbulent free-surface jets illustrating the turbulent structure, the surface current and the nature of the free-surface fluctuations; in addition, the above-mentioned high-Froude-number paradox is discussed. Then, in § 3, the Reynolds-averaged governing equations for free-surface flow are derived. In § 4, the order-of-magnitude analysis of Walker (1997) is applied to the Reynolds-averaged equations to determine the origin of the surface current for arbitrary-Froude-number flows. The inferences arising from the analysis presented in § 4 are shown to be consistent with experimental data in § 5, and the conclusions drawn are summarized in § 6.

2. Background

In this section, some background on observations of free-surface turbulent flows and the surface current is first presented. Experimental data for turbulence quantities and surface elevation statistics are then presented to establish the key aspects of the free-surface jets to be examined.

2.1. *Turbulent free-surface jet spreading*

When a turbulent shear flow such as a jet or a wake evolves near a free surface, a vertically thin region of large transverse (outward) velocity develops adjacent to the surface. This feature, dubbed the *surface current* by Anthony & Willmarth (1992), has been observed in model-ship wakes (Walker & Johnston 1991), free-surface jets (Anthony & Willmarth 1992; Walker, Chen & Willmarth 1995), and wakes of surface-piercing flat plates (Logory, Hirsa & Anthony 1996; Longo, Huang & Stern 1998). Similar behaviour has also been observed in a temporally evolving round jet (Mangiavacchi, Gundlapalli & Akhavan 1994). Thus, the surface current appears to be a ubiquitous feature of turbulent free-surface flows.

The origin of this flow has been the subject of conjecture. Visualization studies have related it to the interaction of tangential vorticity with the free surface (Mangiavacchi *et al.* 1994; Walker *et al.* 1995) as have studies based on near-surface vorticity measurements (Logory *et al.* 1996). Walker *et al.* (1995) proposed that this vortex/free-surface interaction could be related formally to the anisotropy of the turbulence near the free surface. Both Davis & Winarto (1980) and Launder & Rodi (1983) observed similar spreading near the wall in initially axisymmetric wall jets. Launder & Rodi (1983) conjectured that this phenomenon has its origin in the production of streamwise vorticity by Reynolds-stress gradients. The occurrence of similar results in both wall jets and free-surface jets led Anthony & Willmarth (1992) to conclude that the surface current must be caused by the common kinematic boundary condition on the surface-normal velocity (i.e. the surface-normal velocity vanishes at the boundary) not the differing conditions on the tangential velocities.

The study of Walker (1997) examined the evolution of a low-Froude-number jet interacting with a free surface. That study used an order-of-magnitude analysis to determine the leading-order terms in the Reynolds-averaged Navier–Stokes equations

which are responsible for the outward flow in the thin layer adjacent to the surface. The origin of the surface current is traced to terms involving the anisotropy of the turbulence near the free surface – specifically, the normal-stress difference, $(\overline{v^2} - \overline{w^2})$ where w and v represent the vertical and transverse velocity fluctuations, respectively. In that study, it was shown that, near the surface, the transverse momentum equation reduced to

$$\overline{U}\frac{\partial \overline{V}}{\partial x} + \overline{V}\frac{\partial \overline{V}}{\partial y} = -\frac{\partial}{\partial y}(\overline{v^2} - \overline{w^2}), \tag{2.1}$$

where U is the streamwise (x-direction) velocity, V is the horizontal transverse (y-direction) velocity, and the overbar indicates an average quantity. This result indicates that the transverse (outward) flow which develops near the free surface is driven by the gradient in the $(\overline{v^2} - \overline{w^2})$ stress difference. If $\overline{w^2}$ vanishes at the free surface, as required for zero-, or low-Froude-number flows, while $\overline{v^2}$ is unchanged, the transverse flow can develop. If, however, $\overline{w^2}$ and $\overline{v^2}$ are comparable, no transverse flow will develop.

The results of Walker (1997) are consistent with the conjecture of Anthony & Willmarth (1992) which credits the vanishing of the surface-normal velocity W with producing the surface current, as well as those that use the idea of vortex/free-surface interaction (also related to the $W = 0$ condition at the free surface – see Walker 1997). The discussion of Launder & Rodi (1983) in terms of streamwise vorticity seems to be a step removed from the more simple explanation in terms of the momentum equation, and therefore less desirable.

2.2. *Some experimental results for turbulence structure in free-surface jets*

One limitation of the Walker (1997) analysis is that it applies strictly only in the case of zero Froude number. Many of the above-cited observations of the surface current were in moderate- to high-Froude-number flows. At non-zero Froude numbers, the anisotropy which was identified by Walker (1997) as the source of the surface current can be considerably smaller; however, the surface current is not obviously affected. Some other mechanism must therefore drive the surface current in non-zero-Froude-number flows. In this section, some experimental results for free-surface jet flows at equal Reynolds numbers and two different Froude numbers will be presented. The Froude number and Reynolds number are defined in terms of jet-exit velocity and the jet diameter. This will illustrate the similarities in the surface current at low and high Froude number, and the differences in the near-surface anisotropy levels. Measurements of the mean and fluctuating surface elevation level will also be presented.

The experimental results are for two of the jets examined in Walker *et al.* (1995). The data were obtained using a three-component laser velocimeter as described in Walker *et al.* (1995) and the conditions and the instrumentation used are described there in detail; however, the data presented here are more extensive than those in Walker *et al.* (1995). In both cases the jets issued parallel to the free surface, at uniform velocity U_e from a circular nozzle of diameter d, and the jet axis was fixed at $h = 2d$ below the undisturbed free surface. Both jet flows have a Reynolds number $Re = U_e d/\nu = 12\,700$, and the Froude numbers are $Fr = U_e/\sqrt{gd} = 1.0$ and 8.0, where ν is the kinematic viscosity and g is the acceleration due to gravity. The Froude and Reynolds numbers are based on U_e and d. The x-coordinate axis corresponds to the jet axis, increasing in the streamwise direction, with the surface-normal coordinate z positive upward, and the transverse coordinate y defined so that the coordinate

system is right-handed. The origin of the coordinate system is on the jet axis at the exit plane of the jet nozzle. In the following figures, all quantities as normalized with U_e and d. In all the figures, the top edge of the figure indicates the undisturbed free-surface location, $z/d = 2$.

Figure 1 shows the mean streamwise velocity and the mean cross-stream velocity vectors, turbulence kinetic energy and stress anisotropy at $x/d = 16$ for $Fr = 1.0$ and 8.0. The streamwise position corresponds to where the turbulence in the jet has just begun interacting with the free surface. Figures 1(*a*) and 1(*b*) show the mean velocity fields for the two jets. The most striking feature of these images is their similarity. The surface current is apparent in the vector plots, as well as the near-surface spreading of the mean streamwise velocity distributions. For the high-Froude-number case, the velocities associated with the surface current are slightly larger than its low-Froude-number counterpart, while the streamwise velocities are slightly smaller. Figures 1(*c*) and 1(*d*) show the turbulence kinetic energy fields for the two jets. The turbulence level in the high-Froude-number flow (figure 1*d*) is roughly 20% lower than the low-Froude-number flow. This was discussed by Walker *et al.* (1995), where it was proposed that this energy is lost to the generation by the turbulence of waves which radiate the energy away. The final two figures 1(*e*) and 1(*f*) show $(\widehat{v^2} - \widehat{w^2})$, the stress-anisotropy term identified by Walker (1997) as being responsible for the near-surface jet spreading. For the low-Froude-number case (figures 1*e*) the anisotropy is small except near the free surface. It obtains its maximum value near the free surface, above the core of the jet. The anisotropy for the high-Froude-number flow is essentially zero everywhere including the near-surface region. In this figure, the circumflex $\widehat{\ }$ indicates the density-weighted-averaged quantities, equal to time-averaged quantities at locations where fluid density remains constant throughout the averaging period; this type of averaging is introduced below in § 3.

Figure 2 shows the mean streamwise velocity and the mean cross-stream velocity vectors, turbulence kinetic energy and stress anisotropy at $x/d = 32$ for $Fr = 1.0$ and 8.0. The streamwise position corresponds to where the surface current is well established. Figures 2(*a*) and 2(*b*) show the mean velocity fields for the two jets. Again they are very similar, but the high-Froude-number jet exhibits slightly higher streamwise mean velocity; this is probably due to the lower turbulence level and its effect on the jet evolution. Again, the velocities associated with the surface current are slightly larger in the high-Froude-number jet. Figures 2(*c*) and 2(*d*) show the turbulence kinetic energy fields for the two jets. Again, the turbulence level in the high-Froude-number flow (figure 2*d*) is lower than the low-Froude-number flow. Figures 2(*e*) and 2(*f*) show $(\widehat{v^2} - \widehat{w^2})$. For the low-Froude-number case (figure 2*e*) the anisotropy is again small except near the free surface, where it obtains its maximum value, above the core of the jet. Again, the anisotropy for the high-Froude-number flow is essentially zero in the deep portion of the flow, but near the surface, it has risen to nearly 50% of that in the low-Froude-number flow. This is due to the general reduction in the 'local' Froude number associated with the turbulent motions with streamwise distance (owing to the increase in the turbulent lengthscale and the decrease in the turbulent velocity scale).

The foregoing results clearly show that for the low-Froude-number jet, the near-surface stress anisotropy, as characterized by $(\widehat{v^2} - \widehat{w^2})$, is large at both streamwise locations examined, and that there was a significant surface current at both. For the high-Froude-number jet, stress anisotropy is initially very small, and increases with streamwise distance. The surface current, however, is comparable to that in the low-

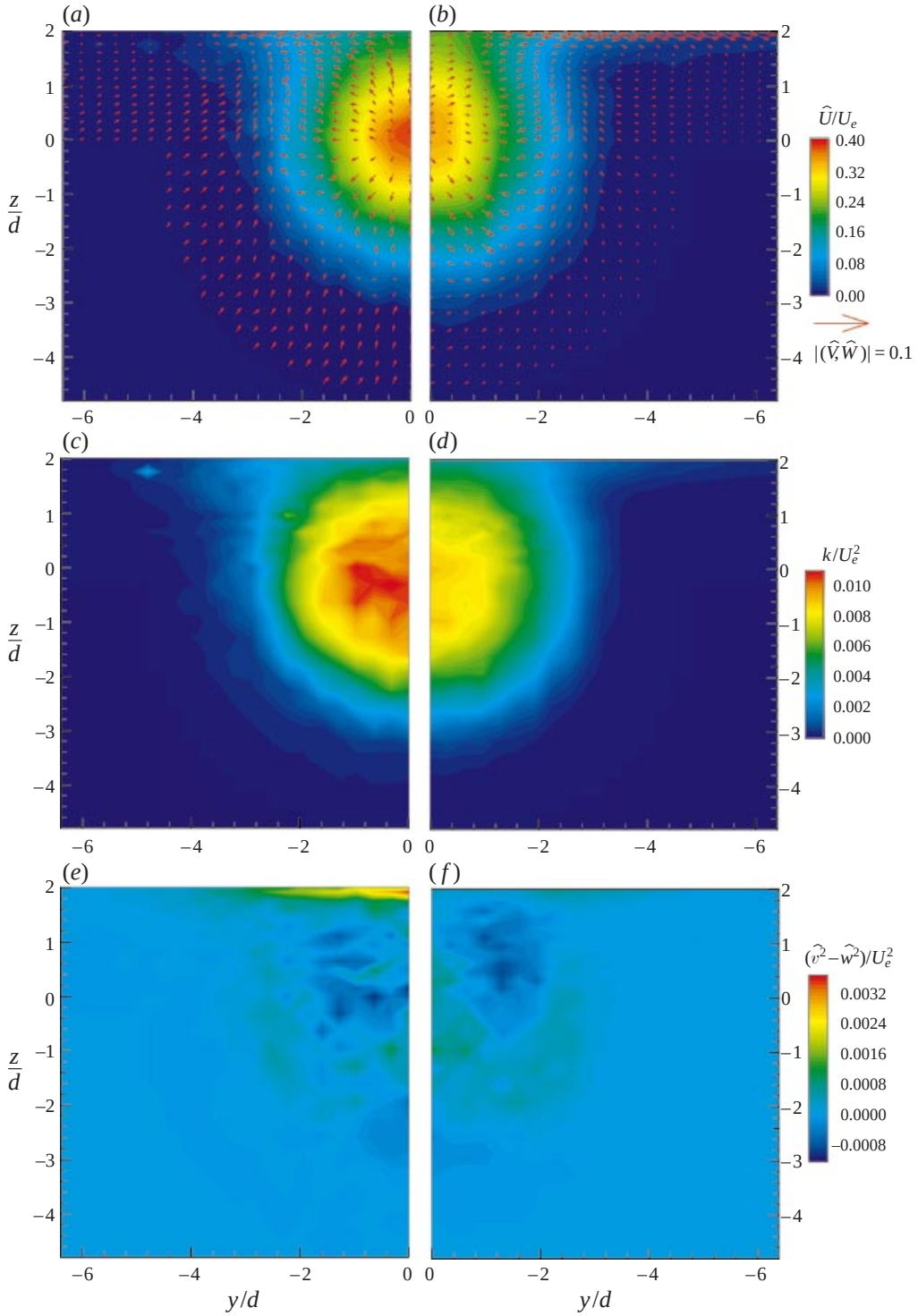

FIGURE 1. Plots of mean streamwise velocity and cross-stream velocity vectors, turbulence kinetic energy level, and stress anisotropy at $x/d = 16$ for $Fr = 1.0$ and 8.0: (*a*) $\widehat{U}/U_e$ and $(\widehat{V}, \widehat{W})$ vectors for $Fr = 1.0$; (*b*) $\widehat{U}/U_e$ and $(\widehat{V}, \widehat{W})$ vectors for $Fr = 8.0$; (*c*) k/U_e^2 for $Fr = 1.0$; (*d*) k/U_e^2 for $Fr = 8.0$; (*e*) $(\widehat{v^2} - \widehat{w^2})/U_e^2$ for $Fr = 1.0$; (*f*) $(\widehat{v^2} - \widehat{w^2})/U_e^2$ for $Fr = 8.0$.

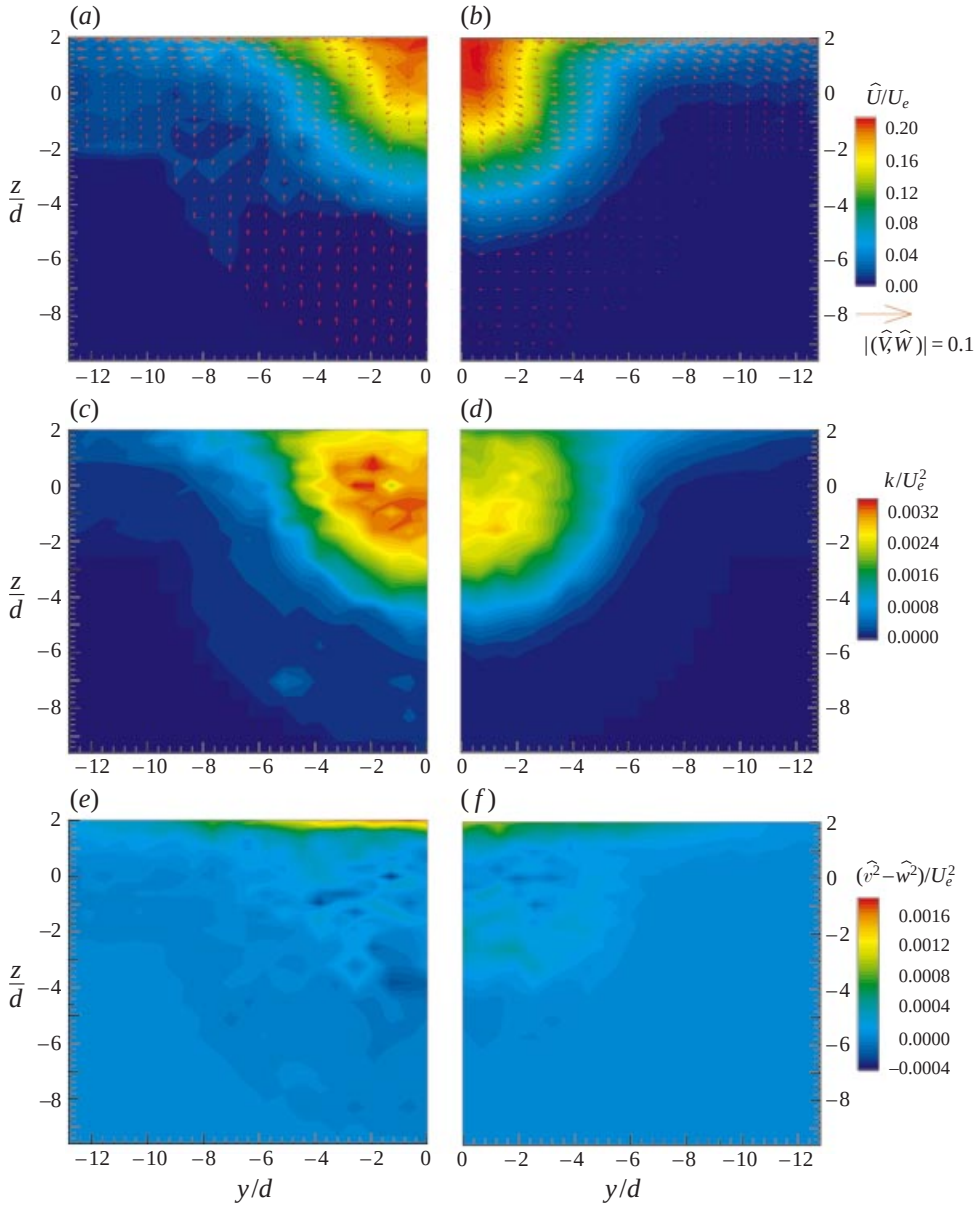

FIGURE 2. Plots of mean streamwise velocity and cross-stream velocity vectors, turbulence kinetic energy level, and stress anisotropy at $x/d = 32$ for $Fr = 1.0$ and 8.0: (*a*) $\widehat{U}/U_e$ and $(\widehat{V}, \widehat{W})$ vectors for $Fr = 1.0$; (*b*) $\widehat{U}/U_e$ and $(\widehat{V}, \widehat{W})$ vectors for $Fr = 8.0$; (*c*) k/U_e^2 for $Fr = 1.0$; (*d*) k/U_e^2 for $Fr = 8.0$; (*e*) $(\widehat{v^2} - \widehat{w^2})/U_e^2$ for $Fr = 1.0$; (*f*) $(\widehat{v^2} - \widehat{w^2})/U_e^2$ for $Fr = 8.0$.

Froude-number flow (actually larger). Hence, the argument put forth by Walker (1997) that the stress anisotropy is the cause of the near-surface jet spreading can at best explain the behaviour of the low-Froude-number flow. This is not surprising, since that analysis applies strictly only at $Fr = 0$. At high Froude number, an additional mechanism must be at work. The nature of this additional mechanism can be seen in the equations for Reynolds-averaged flow with a deformable free surface (to be

derived below). It derives from the integrated effect of the pressure forces acting on the fluctuating free surface. As a result, it appears that the free-surface fluctuations play a key role in high-Froude-number jet spreading; surface elevation statistics will be discussed next.

2.3. *Surface elevation measurements*

A laser-induced-fluorescence-based wave probe system was used to measure the surface elevation. This is similar to that used by Duncan (1993) in his study of stationary breaking waves. In this method, a fluorescent dye (Fluorescein disodium salt) is added to the water at low concentration. A collimated laser beam oriented perpendicular to the water surface enters from above. The beam was roughly 1 mm in diameter at the free surface. The laser energy absorbed and re-emitted as fluorescence yields a bright emission from the laser beam for the region below the free surface. The laser beam is not visible above the free surface. The resulting step change in intensity at the free surface is observed using a high-speed line-scan camera (EG&G Reticon Model LC1912) connected to a Pentium-based computer. For $Fr = 8.0$, the laser beam was imaged using a 70 mm lens, focused at infinity, with a +3 dioptre close-up lens. The resulting resolution of the surface elevation measurements is about 50 μm. For $Fr = 1.0$, the surface fluctuations are much smaller and the 70 mm lens was used in conjunction with an extension tube of about 1 m for a tenfold increase in resolution.

The mean and r.m.s. surface elevation for each position were calculated using ensembles of 1000 independent measurements. For $Fr = 8.0$, the averaging time for each measurement is 1 ms and, for $Fr = 1.0$, 64 ms. The sampling rate in both cases was 1 Hz. The intensity profiles were digitized and stored in the computer. The digitized profiles were processed and the position of the water–air interface was determined using calibration data. In the high-Froude-number case, we observed a sharp transition in light intensity at the air–water interface, and the free surface was defined as the position of maximum light intensity gradient. For the low-Froude-number case, because of the high magnification used, the transition was more gradual, and the intensity data was noisier. For this case, the free-surface position was defined as the location where the light intensity was 45% of the maximum intensity (this latter approach is slightly less accurate for clean data, but more immune to noise).

The significant regions of the free surface were mapped with the above-described system. For $Fr = 8.0$, measurements covered a region from $x/d = 4$ to 38. The horizontal extent of the measurements increased linearly with x so that $y/x = 0.4$. For $Fr = 1.0$, the region from $x/d = 4$ to 26 was similarly covered.

Figures 3(*a*) and 3(*b*) show the r.m.s. surface-fluctuation level η'/d for $Fr = 1.0$ and 8.0, respectively. The η' levels for the high-Froude-number flow are clearly more than an order of magnitude larger than those for the low-Froude-number flow. For $Fr = 8.0$, the maximum in η' occurs at about $x/d = 20$ and extends about $12d$ in the streamwise x-direction and about $2d$ in the transverse y-direction. The maximum occurs above the jet axis, and η' decreases monotonically with increasing y. For $Fr = 1.0$, the maximum occurs above the jet axis at about $x/d = 12$, and the peak is much lower and extends over a much smaller streamwise and lateral extent.

Figures 4(*a*) and 4(*b*) show the mean surface-elevation $\overline{\eta}/d$ for $Fr = 1.0$ and 8.0, respectively. For the high-Froude-number flow (figure 4*b*), the mean free-surface elevation is similar to the r.m.s. surface elevation, shown above, with the peak located above the jet axis at about $x/d = 20$, with comparable lateral extent of the peak region, but with a streamwise extent of about half that of the peak in the r.m.s. surface

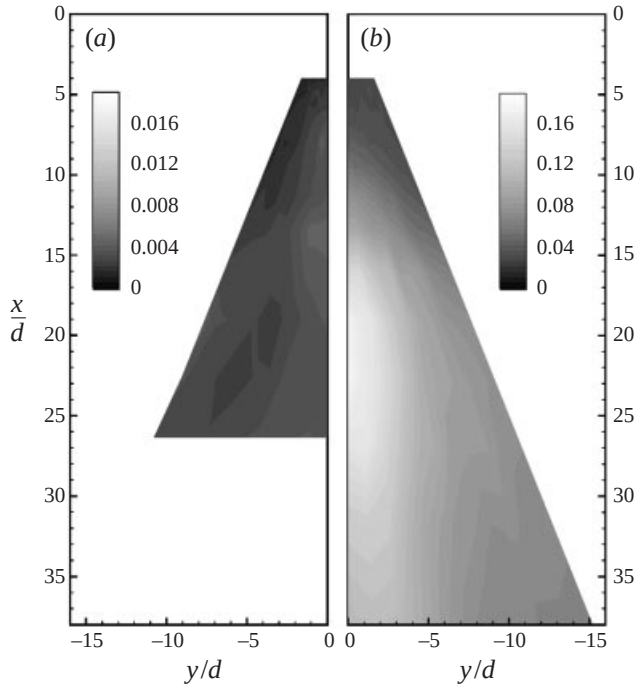

FIGURE 3. Plots of r.m.s of surface elevation fluctuation η'/d for (*a*) $Fr = 1.0$, and (*b*) $Fr = 8.0$. Note that the range for (*a*) is one-tenth that for (*b*).

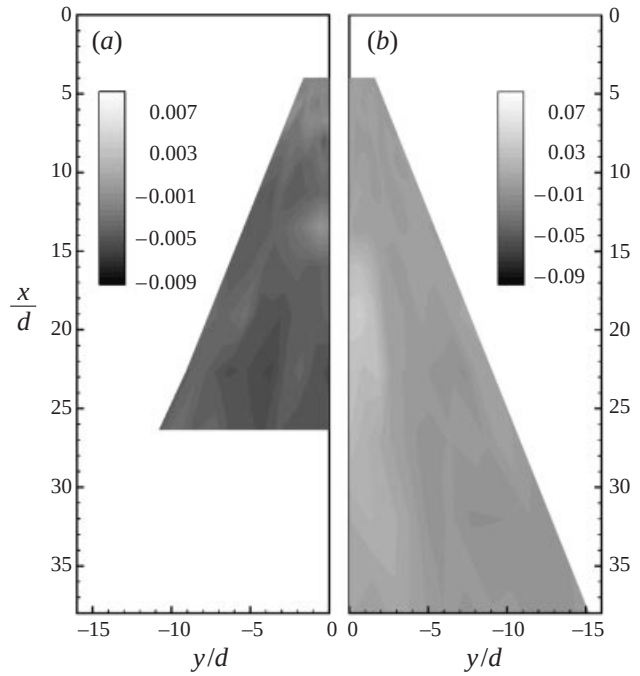

FIGURE 4. Plots of mean surface elevation $\overline{\eta}/d$ for (*a*) $Fr = 1.0$, and (*b*) $Fr = 8.0$. Note that the range for (*a*) is one-tenth that for (*b*).

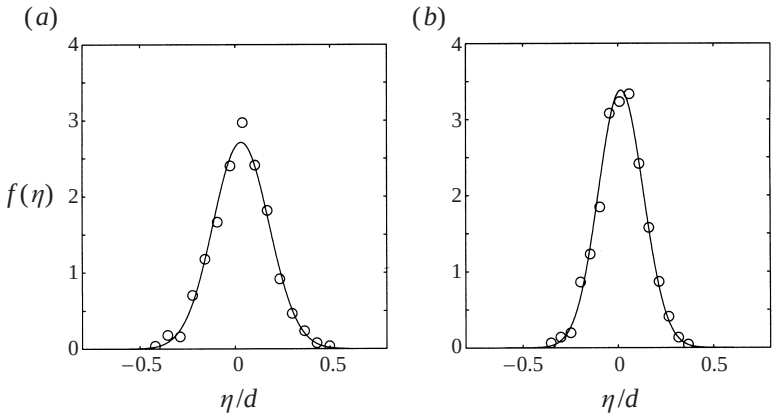

FIGURE 5. Probability density functions for surface elevation η/d above the jet axis at (*a*) $x/d = 16$ and (*b*) $x/d = 32$: ○, experimental data; ———, Gaussian distribution with mean and standard deviation of experimental data.

elevation. The maximum mean surface elevation is about 20% of the maximum r.m.s. surface elevation, and the mean surface slopes are of the order of 10^{-2}. For the low-Froude-number case (figure 4*a*), the mean free-surface deflection is nearly two orders of magnitude smaller than that for the high-Froude-number flow.

The probability density function (p.d.f.) of the free-surface position $f(\eta)$ will be central to some results in later sections. For the low-Froude-number flow, the surface elevation fluctuations are almost negligibly small, and so only the high-Froude-number case will be examined. The p.d.f. of η for two streamwise positions, $x/d = 16$ and 32, above the jet axis $y = 0$ are shown in figures 5(*a*) and 5(*b*), respectively. Also shown in each figure is a Gaussian distribution with the experimentally determined mean and standard deviation for the data. From this comparison, it is clear that the distributions are nearly Gaussian.

2.4. *Summary*

The foregoing results show that, for high-Froude-number flows, the surface current occurs even though the anisotropy which characterizes low-Froude-number flows is absent, or much reduced. The results of Walker (1997) would indicate a decrease in the surface-current velocities with decreasing anisotropy. The main reason for this discrepancy is that Walker (1997) began with the conventional RANS equations, with the free-surface boundary conditions applied at the undisturbed free-surface location. As was discussed in Walker (1997), this is appropriate only for low-Froude-number flows where there are no significant, unsteady free-surface deformations. For high-Froude-number flows, the conventional RANS equations are inappropriate, because the position of the free surface is not well defined at high Froude number as a result of the unsteady surface deformations. Therefore, the conclusion that the surface current results from the stress-anisotropy is not general, and cannot be applied *a priori* to high-Froude-number flows. The experimental results presented above are evidence that this extension of the results of Walker (1997) to high-Froude-number flows cannot be made.

One of the objectives of this study is to establish the origin of the surface current for high-Froude-number flows in much the same way as Walker (1997) did for zero- or low-Froude-number flows. A key requirement for the solution of this problem is

a form of the Reynolds-averaged equations of motion which both admits surface deformations, and handles them in a rigorous way. This is the other objective of the study, and is discussed next.

3. The governing equations

In this section, a Reynolds-averaged form of the Navier–Stokes equations which admits unsteady, turbulent surface deformations is developed. The resulting equations are similar in character to the level-set formulation of Chang *et al.* (1996). The basis for the equations is the Navier–Stokes equations for variable-property, incompressible, Newtonian flow. First, it is shown that these equations actually contain both the equations of motion and the interfacial boundary conditions for immiscible two-fluid flow. The resulting equations are then time-averaged to yield the appropriate form of the governing equations for the mean flow.

3.1. *The governing equations for the instantaneous flow*

Any attempt to derive the appropriate Reynolds-averaged form of the governing equations must start from a set of equations which are able to represent the flow accurately. We wish to time average the flow at a point in space while keeping track of which phase is present; hence, the equations that are averaged must be applicable to the entire region of interest – the region above the free surface as well as below. The region above the free surface is usually a gas phase, such as air or water vapour, or, in the case of a classical free surface, it is a void with zero density, viscosity, and pressure.

It will now be established that the appropriate governing equations for a two-fluid domain are the Navier–Stokes equations, written for non-constant fluid properties (since the two fluids have different properties), and applied across the entire domain, including the interface. It will be shown that these general equations can be reduced to the constant property equations applied in the interior of the two fluid domains and an appropriate set of boundary conditions applied at the interface. The continuity equation for non-constant property fluids is given by

$$\frac{\partial \rho}{\partial t} + \frac{\partial}{\partial x_i}(\rho U_i) = 0, \tag{3.1}$$

and momentum conservation is represented by

$$\frac{\partial}{\partial t}(\rho U_i) + \frac{\partial}{\partial x_j}(\rho U_j U_i) = -\frac{\partial P}{\partial x_i} + \frac{\partial}{\partial x_j}\left[\mu\left(\frac{\partial U_i}{\partial x_j} + \frac{\partial U_j}{\partial x_i}\right)\right] + \rho g_i. \tag{3.2}$$

Also, in incompressible flow, ρ is constant for a fluid particle, hence

$$\frac{\mathrm{D}\rho}{\mathrm{D}t} = \frac{\partial \rho}{\partial t} + U_i \frac{\partial \rho}{\partial x_i} = 0. \tag{3.3}$$

Subtracting (3.3) from (3.1) yields

$$\frac{\partial U_i}{\partial x_i} = 0. \tag{3.4}$$

Equations (3.1) to (3.4) all apply over the entire two-fluid domain.

A level-set function $H(x_i, t)$ can be defined on the entire domain so that the two fluids are separated by an interface corresponding to the level set

$$H(x_i, t) = 0. \tag{3.5}$$

Here, $H < 0$ is the region occupied by fluid 0 and $H > 0$ indicates the region occupied by fluid 1. To keep track of the fluid properties at the point of interest, an indicator function $I_\circ(x_i, t)$, a unit step function, is defined to be unity in fluid 0 and zero in fluid 1, i.e.

$$\begin{aligned} I_\circ &= 1 \quad \text{for} \quad H(x_i, t) < 0 \\ &= 0 \quad \text{for} \quad H(x_i, t) > 0. \end{aligned} \tag{3.6}$$

Since $I_\circ$ is a unit step function which depends on H,

$$\frac{\partial I_\circ}{\partial x_i} = -\frac{\partial H}{\partial x_i}\delta(H), \quad \frac{\partial I_\circ}{\partial t} = -\frac{\partial H}{\partial t}\delta(H), \tag{3.7}$$

where δ is the Dirac delta function. A complementary indicator function $I_1 = 1 - I_\circ$ is also defined which indicates the second fluid domain.

The continuity equation (3.1) can be written explicitly, rather than implicitly, for both fluid regions by recognizing the change in density:

$$\frac{\partial}{\partial t}(\rho_\circ I_\circ + \rho_1 I_1) + \frac{\partial}{\partial x_i}\{(\rho_\circ I_\circ + \rho_1 I_1) U_i\} = 0, \tag{3.8}$$

where $\rho_\circ$ and ρ_1 are the fixed densities of the two fluids in the regions identified by $I_\circ$ and I_1, respectively. (Here, it is assumed that the velocities are continuous across the interface.) Expanding the derivatives and rearranging yields

$$\begin{aligned} &\left\{\frac{\partial \rho_\circ}{\partial t} + \frac{\partial}{\partial x_i}(\rho_\circ U_i)\right\} I_\circ + \rho_\circ\left(\frac{\partial I_\circ}{\partial t} + U_i\frac{\partial I_\circ}{\partial x_i}\right) \\ &\qquad + \left\{\frac{\partial \rho_1}{\partial t} + \frac{\partial}{\partial x_i}(\rho_1 U_i)\right\} I_1 + \rho_1\left(\frac{\partial I_1}{\partial t} + U_i\frac{\partial I_1}{\partial x_i}\right) = 0. \end{aligned} \tag{3.9}$$

Making use of (3.7) and recognizing that $\rho_\circ$ and ρ_1 are constants yields

$$\left\{\rho_\circ\frac{\partial U_i}{\partial x_i}\right\} I_\circ + \left\{\rho_1\frac{\partial U_i}{\partial x_i}\right\} I_1 + (\rho_1 - \rho_\circ)\left\{\frac{\partial H}{\partial t} + U_i\frac{\partial H}{\partial x_i}\right\}\delta(H) = 0. \tag{3.10}$$

The three sets of terms in brackets apply in the two fluids, and at the interface, respectively. The first two terms are just the constant-density continuity equations written for the fluid regions as indicated by $I_\circ$ and I_1. The third term is usually called the kinematic boundary condition, and is the expression of mass conservation at the interface; i.e. no mass may cross the interface. Since $I_\circ$ and I_1 are non-zero in mutually exclusive regions in space, and $\delta(H)$ is non-zero only on the boundary between the two regions, the collections of terms multiplying $I_\circ$, I_1 and $\delta(H)$ must vanish independently. Hence,

$$\frac{\partial U_i}{\partial x_i} = 0 \tag{3.11}$$

in either fluid, and

$$\frac{\partial H}{\partial t} + U_i\frac{\partial H}{\partial x_i} = 0 \tag{3.12}$$

on the interface, where $H(x_i, t) = 0$.

The momentum equations can be treated in a similar fashion. Writing (3.2) while explicitly recognizing the two fluid regions yields

$$\frac{\partial}{\partial t}\{(\rho_\circ I_\circ + \rho_1 I_1)U_i\} + \frac{\partial}{\partial x_j}\{(\rho_\circ I_\circ + \rho_1 I_1)U_j U_i\} = -\frac{\partial}{\partial x_i}(P_\circ I_\circ + P_1 I_1) + \frac{\partial}{\partial x_j}\left[(\mu_\circ I_\circ + \mu_1 I_1)\left(\frac{\partial U_i}{\partial x_j} + \frac{\partial U_j}{\partial x_i}\right)\right] + (\rho_\circ I_\circ + \rho_1 I_1)g_i. \quad (3.13)$$

This form of this equation assumes continuity in the velocities across the fluid interface, but admits step changes in fluid properties and pressure across the interface. (For non-trivial viscous flows, there will, in general, be a step change in pressure at the interface; only in inviscid flows is the pressure required to be continuous across the interface.) Expanding the derivatives and collecting terms yields

$$\rho_\circ\left(\frac{\partial U_i}{\partial t} + U_j\frac{\partial U_i}{\partial x_j}\right)I_\circ + \rho_1\left(\frac{\partial U_i}{\partial t} + U_j\frac{\partial U_i}{\partial x_j}\right)I_1 = \left\{-\frac{\partial P_\circ}{\partial x_i} + \frac{\partial}{\partial x_j}\left[\mu_\circ\left(\frac{\partial U_i}{\partial x_j} + \frac{\partial U_j}{\partial x_i}\right)\right] + \rho_\circ g_i\right\}I_\circ + \left\{-\frac{\partial P_1}{\partial x_i} + \frac{\partial}{\partial x_j}\left[\mu_1\left(\frac{\partial U_i}{\partial x_j} + \frac{\partial U_j}{\partial x_i}\right)\right] + \rho_1 g_i\right\}I_1 - \left\{-P_\circ\delta_{ij} + \mu_\circ\left(\frac{\partial U_i}{\partial x_j} + \frac{\partial U_j}{\partial x_i}\right) + P_1\delta_{ij} - \mu_1\left(\frac{\partial U_i}{\partial x_j} + \frac{\partial U_j}{\partial x_i}\right)\right\}\frac{\partial H}{\partial x_j}\delta(H), \quad (3.14)$$

where δ_{ij} is the Kronecker delta. Again, the collections of terms multiplying $I_\circ$, I_1 and $\delta(H)$ must vanish independently. This requires that

$$\rho\left(\frac{\partial U_i}{\partial t} + U_j\frac{\partial U_i}{\partial x_j}\right) = -\frac{\partial P}{\partial x_i} + \frac{\partial}{\partial x_j}\left[\mu\left(\frac{\partial U_i}{\partial x_j} + \frac{\partial U_j}{\partial x_i}\right)\right] + \rho g_i \quad (3.15)$$

in the regions defined by $I_\circ$ and I_1, and that

$$-P_\circ\delta_{ij} + \mu_\circ\left(\frac{\partial U_i}{\partial x_j} + \frac{\partial U_j}{\partial x_i}\right) = -P_1\delta_{ij} + \mu_1\left(\frac{\partial U_i}{\partial x_j} + \frac{\partial U_j}{\partial x_i}\right) \quad (3.16)$$

on the boundary defined by $H(x_i, t) = 0$. This recovers the conventional form for the momentum equations and the appropriate boundary conditions for the interface for a two-fluid problem. For a flow with constant properties and no surface tension (surface tension is discussed next), the momentum equations are given by (3.15), the continuity equation is (3.11) and the kinematic and dynamic boundary conditions are given by (3.12) and (3.16), respectively. Hence, the general governing equations (3.1) and (3.2) embody both the constant property forms of the equations and the boundary conditions and can therefore be applied across the entire fluid domain, including the interface. This represents a formal justification of the level-set approach to interfacial flow described by Chang *et al.* (1996) and others.

While it demonstrates that the variable-property Navier–Stokes equations can be applied to a two-fluid domain, the foregoing derivation does not include surface tension. The reason is that surface tension is not a continuum effect, and therefore is not included in the continuum equations. The surface tension is, however, readily incorporated into the dynamic boundary condition (3.16). Having done this, one can then work 'backward' to the appropriate form of the Navier–Stokes equations for the two-fluid problem which incorporates surface tension. In addition, it is often more convenient to use a pressure with the hydrostatic contribution removed ('piezometric' pressure), which can be incorporated in a similar fashion. These are discussed next.

For a stationary fluid ($U_i = 0$), a difference in pressure between the two fluids

can arise owing to the effects of surface tension. These non-continuum effects are not represented in the continuum equations. Owing to surface tension, there will be an increase in the pressure which is proportional to the curvature of the surface $\Delta P = \gamma/R$, where R is the local radius of curvature of the interface ($R^{-1} = R_1^{-1} + R_2^{-1}$, where R_1 and R_2 are the principal radii of curvature of the free surface, Batchelor 1967). R is taken to be positive when the centre of curvature lies in the region defined by $I_\circ(x_i, t)$. Written in terms of $H(x_i, t)$ (after Aris 1962), the curvature is given by

$$\frac{1}{R} = \frac{\partial^2 H}{\partial x_k \partial x_l}\left[\frac{\partial H}{\partial x_k}\frac{\partial H}{\partial x_l} - \left(\frac{\partial H}{\partial x_m}\frac{\partial H}{\partial x_m}\right)\delta_{kl}\right]\left(\frac{\partial H}{\partial x_m}\frac{\partial H}{\partial x_m}\right)^{-3/2}$$
$$= \frac{\partial^2 H}{\partial x_k \partial x_l}\left[n_k n_l - \delta_{kl}\right]\left(\frac{\partial H}{\partial x_m}\frac{\partial H}{\partial x_m}\right)^{-1/2}, \tag{3.17}$$

evaluated at $H(x_i, t) = 0$. Here, n_i is the unit normal vector. If we consider only the case of small slope surface slope $n_i \approx (\alpha, \beta, 1)$ where α and β are small parameters, then (3.17) reduces to

$$\frac{1}{R} \approx -\frac{\partial^2 H}{\partial x_k \partial x_k}\left(\frac{\partial H}{\partial x_m}\frac{\partial H}{\partial x_m}\right)^{-1/2}. \tag{3.18}$$

Sometimes, the governing Navier–Stokes equations are written in terms of the piezometric pressure, $P' = P + \rho g z$ where $g^2 = g_i g_i$, and g_i is assumed to point in the $-z$-direction. This is helpful when considering the effects of large gravity forces (near-zero Froude number) because it eliminates from the governing equations the body force term, which can overwhelm the other terms. The body force term then appears in the boundary condition where it is easier to accommodate. Incorporating the piezometric pressure P', and the surface tension above into (3.15), yields

$$\rho\left(\frac{\partial U_i}{\partial t} + U_j\frac{\partial U_i}{\partial x_j}\right) = -\frac{\partial P'}{\partial x_i} + \frac{\partial}{\partial x_j}\left[\mu\left(\frac{\partial U_i}{\partial x_j} + \frac{\partial U_j}{\partial x_i}\right)\right] \tag{3.19}$$

for the momentum equations, and

$$-\left(P_1' - \rho_1 g z\right)\delta_{ij} + \mu_1\left(\frac{\partial U_i}{\partial x_j} + \frac{\partial U_j}{\partial x_i}\right) = -\left(P_\circ' + \frac{\gamma}{R} - \rho_\circ g z\right)\delta_{ij} + \mu_\circ\left(\frac{\partial U_i}{\partial x_j} + \frac{\partial U_j}{\partial x_i}\right), \tag{3.20}$$

evaluated on the surface $H(x_i, t) = 0$, for the boundary condition.

These equations and boundary conditions for the two-fluid problem, written in terms of the piezometric pressure and including surface tension, are equivalent to the following set of equations for the explicit continuum formulation

$$\frac{\partial}{\partial t}\left\{\left(\rho_\circ I_\circ + \rho_1 I_1\right) U_i\right\} + \frac{\partial}{\partial x_j}\left\{\left(\rho_\circ I_\circ + \rho_1 I_1\right) U_j U_i\right\} = -\frac{\partial}{\partial x_i}\left(P_\circ' I_\circ + P_1' I_1\right)$$
$$+\frac{\partial}{\partial x_j}\left[\left(\mu_\circ I_\circ + \mu_1 I_1\right)\left(\frac{\partial U_i}{\partial x_j} + \frac{\partial U_j}{\partial x_i}\right)\right] + \left[\left(\rho_1 - \rho_\circ\right) g z + \frac{\gamma}{R}\right]\frac{\partial H}{\partial x_i}\delta(H). \tag{3.21}$$

The implicit continuum form will be

$$\frac{\partial}{\partial t}\left(\rho U_i\right) + \frac{\partial}{\partial x_j}\left(\rho U_j U_i\right) = -\frac{\partial}{\partial x_i}P' + \frac{\partial}{\partial x_j}\left[\mu\left(\frac{\partial U_i}{\partial x_j} + \frac{\partial U_j}{\partial x_i}\right)\right]$$
$$+\left[\left(\rho_1 - \rho_\circ\right) g z + \frac{\gamma}{R}\right]\frac{\partial H}{\partial x_i}\delta(H), \tag{3.22}$$

where $\rho = \rho_\circ I_\circ + \rho_1 I_1$, and similarly for viscosity and pressure. These differ from (3.2),

above, via the inclusion of surface tension and the use of the piezometric pressure P'. These equations are equivalent to those used by Chang *et al.* (1996) as the basis for their level-set method for interface problems.

3.2. *The governing equations for the time-averaged flow*

To describe the mean behaviour of turbulent flows, the governing equations for the instantaneous flows can be time averaged. For two-fluid flows, separated by an assumed stationary interface, the time-averaging process is usually applied to the equations for the individual phases, and to the boundary conditions. For turbulent flows, where the boundary location is inherently unsteady, that approach cannot be implemented, since the boundary motions cannot be incorporated. Using the continuity equation (3.1) and the momentum equation (3.22), which apply to the entire field, the averaging process can be carried out in a rigorous way, accounting for the unsteady motions in the free surface.

The continuity and momentum equations will be averaged in time. For this purpose, the time average is defined as

$$\overline{Q}(x_i,t) = \frac{1}{T}\int_0^T Q(x_i,t)\,\mathrm{d}t. \tag{3.23}$$

It is assumed that the averaging time T will be much longer than the timescale for the turbulent fluctuations, but much shorter than the timescale for the variation of the mean flow (after Hinze 1975, pp. 6 and 20). Applying this averaging to either indicator function yields the fraction of time F that the given fluid is present

$$\frac{1}{T}\int_0^T \{I_\circ(x_i,t) + I_1(x_i,t)\}\,\mathrm{d}t = F_\circ(x_i,t) + F_1(x_i,t) = 1. \tag{3.24}$$

Applying this average to a fluid property, say the density ρ, yields

$$\begin{aligned}\overline{\rho}(x_i,t) &= \frac{1}{T}\int_0^T \{\rho_\circ I_\circ(x_i,t) + \rho_1 I_1(x_i,t)\}\,\mathrm{d}t \\ &= \rho_\circ F_\circ(x_i,t) + \rho_1 F_1(x_i,t).\end{aligned} \tag{3.25}$$

Substituting the continuity equation (3.1) into the definition of the time average (3.23) yields

$$\frac{\partial \overline{\rho}}{\partial t} + \frac{\partial}{\partial x_i}\left(\overline{\rho U}_i\right) = 0. \tag{3.26}$$

If we define a density-weighted average $\widehat{U}_i$ such that

$$\overline{\rho}\ \widehat{U}_i = \overline{\rho U}_i, \tag{3.27}$$

then the average continuity equation becomes

$$\frac{\partial \overline{\rho}}{\partial t} + \frac{\partial}{\partial x_i}\left(\overline{\rho}\ \widehat{U}_i\right) = 0. \tag{3.28}$$

This density-weighted average, is essentially the Favre-average discussed by Hinze (1975, p. 21), and is often used for compressible flows (see e.g. Blaisdell 1991). Note that, at locations where fluid density is constant throughout the averaging period, density-weighted average is equal to the time average.

For the instantaneous flow, the kinematic free-surface boundary condition (3.12) is used as an evolution equation for the interface. It was shown above that this

follows directly from the continuity equation. Similarly, an evolution equation for the mean free-surface location can be obtained from the averaged continuity equation. Expanding the time-averaged continuity equation yields

$$0 = \frac{\partial \overline{\rho}}{\partial t} + \frac{\partial}{\partial x_i}\left(\overline{\rho}\widehat{U}_i\right) = \left(\frac{\partial}{\partial t} + \widehat{U}_i\frac{\partial}{\partial x_i}\right)\overline{\rho} + \overline{\rho}\frac{\partial \widehat{U}_i}{\partial x_i}, \tag{3.29}$$

for $\overline{\rho} = \rho_\circ F_\circ + \rho_1 F_1 = (\rho_\circ - \rho_1)F_\circ + \rho_1$, $\partial\overline{\rho}/\partial x_i = (\rho_\circ - \rho_1)\partial F_\circ/\partial x_i$. If we define $G(x_i, t)$ such that $F_\circ = F_\circ(G)$ only, then

$$\frac{\partial F_\circ}{\partial x_i} = -\frac{\partial G}{\partial x_i} f(G), \tag{3.30}$$

where $f(G) = -\partial F_\circ/\partial G$ (and similarly for $\partial F_\circ/\partial t$). Since $F_\circ(x_i, t)$ is the probability of occurrence of the fluid indicated by $I_\circ$ at the given location (i.e. one minus the cumulative probability density function for the free-surface position), $f(G)$ can be interpreted as the p.d.f. of the free-surface position, and $G(x_i, t)$ as the normalized distance from the mean free-surface position (normalized so that the level curves of G are lines of constant probability). Equation (3.29) can then be written as

$$0 = \left\{\rho_\circ \frac{\partial \widehat{U}_i}{\partial x_i}\right\} F_\circ + \left\{\rho_1 \frac{\partial \widehat{U}_i}{\partial x_i}\right\} F_1 + (\rho_1 - \rho_\circ)\left\{\frac{\partial G}{\partial t} + \widehat{U}_i\frac{\partial G}{\partial x_i}\right\} f(G), \tag{3.31}$$

analogous to (3.10), or, in more compact form, as

$$0 = \left(\frac{\partial G}{\partial t} + \widehat{U}_i\frac{\partial G}{\partial x_i}\right) f(G) - \frac{\overline{\rho}}{\rho_\circ - \rho_1}\frac{\partial \widehat{U}_i}{\partial x_i}. \tag{3.32}$$

This expression is the Reynolds-averaged equivalent of the kinematic boundary condition, and can be thought of as an evolution equation for the mean free surface. For time-averaged flows, G is analogous to H for the instantaneous flows; however, G is defined in a slightly more restrictive fashion. This expression recognizes that the free-surface location is 'fuzzy' in turbulent flows; it applies to the region where $f(G)$ is non-zero, but not at a specific location, since the instantaneous free-surface position fluctuates. For the case where there are no free-surface fluctuations $f(G) = \delta(G)$ and the divergence of $\widehat{U}_i$ goes to zero. Under these conditions (3.32) reverts to (3.12) and $G(x_i, t)$ is effectively $H(x_i, t)$.

Attention is now turned to the momentum equation. If we define a Reynolds-type decomposition $U_i = \widehat{U}_i + u_i$ then, the left-hand side of the momentum equation (3.22) is easily averaged to yield

$$\frac{\partial}{\partial t}\left(\overline{\rho}\ \widehat{U}_i\right) + \frac{\partial}{\partial x_j}\left(\overline{\rho}\ \widehat{U}_j\ \widehat{U}_i\right) + \frac{\partial}{\partial x_j}\left(\overline{\rho}\ \widehat{u_j u_i}\right) = \overline{\rho}\left[\frac{\partial \widehat{U}_i}{\partial t} + \widehat{U}_j\frac{\partial \widehat{U}_i}{\partial x_j}\right] + \frac{\partial}{\partial x_j}\left(\overline{\rho}\ \widehat{u_j u_i}\right). \tag{3.33}$$

The average of the right-hand side of the momentum equation (3.22), excluding the terms multiplied by $\delta(H)$, is

$$-\frac{\partial}{\partial x_i}\overline{P'} + \frac{\partial}{\partial x_j}\left(\overline{\mu S_{ij}}\right), \tag{3.34}$$

where S_{ij} is the strain rate, defined as

$$S_{ij} = \frac{\partial U_i}{\partial x_j} + \frac{\partial U_j}{\partial x_i}. \tag{3.35}$$

The average viscous stress, in the second term in (3.34), can be written as

$$\begin{aligned}\overline{\mu S_{ij}} &= \overline{\mu}\widehat{S}_{ij} + \langle \mu S_{ij} \rangle \\ &= \overline{\mu}\left[\frac{\partial \widehat{U}_i}{\partial x_j} + \frac{\partial \widehat{U}_j}{\partial x_i}\right] + \overline{\mu}\left[\widehat{\frac{\partial u_i}{\partial x_j}} + \widehat{\frac{\partial u_j}{\partial x_i}}\right] + \langle \mu S_{ij} \rangle,\end{aligned} \tag{3.36}$$

where

$$\langle \mu S_{ij} \rangle = \frac{1}{\overline{\rho}}(\rho_1 \mu_\circ - \rho_\circ \mu_1)\left[\frac{1}{T}\int_0^T (F_1 I_\circ - F_\circ I_1)\, S_{ij}\, \mathrm{d}t\right]. \tag{3.37}$$

The term $\langle \mu S_{ij} \rangle$ has the property that it will vanish when either $\rho_\circ = \mu_\circ = 0$, $\rho_1 = \mu_1 = 0$, or at positions far removed from the interface where the density is constant, as indicated by either $F_\circ = 0$ and $I_\circ = 0$, or $F_1 = 0$ and $I_1 = 0$. The $\rho_1 = 0$, $\mu_1 = 0$ case corresponds to the classical free-surface situation.

The last term in (3.22), that containing $\delta(H)$, represents the fluctuating surface forces and is averaged to yield

$$\frac{1}{T}\int_0^T \left[(\rho_1 - \rho_\circ)\, gz + \frac{\gamma}{R}\right]\frac{\partial H}{\partial x_i}\delta(H)\mathrm{d}t = (\rho_1 - \rho_\circ) g z \overline{\frac{\partial H}{\partial x_i}\delta(H)} + \gamma \overline{\frac{\partial H}{\partial x_i}\frac{\delta(H)}{R}}. \tag{3.38}$$

By rewriting the terms involving $(\partial H/\partial x_i)\delta(H)$ in terms of $I_\circ$ prior to averaging, it can be shown that (3.38) yields

$$\frac{1}{T}\int_0^T \left[(\rho_1 - \rho_\circ)\, gz + \frac{\gamma}{R}\right]\frac{\partial H}{\partial x_i}\delta(H)\mathrm{d}t = \left[(\rho_1 - \rho_\circ)\, gz + \frac{\gamma}{\langle R \rangle}\right]\frac{\partial G}{\partial x_i} f(G), \tag{3.39}$$

where $\langle R(x_i, t) \rangle^{-1}$ is the 'effective' mean surface curvature given by

$$\frac{1}{\langle R \rangle} = \overline{\frac{\partial H}{\partial x_i}\frac{\delta(H)}{R}}\frac{\partial G}{\partial x_i}\left[\left(\frac{\partial G}{\partial x_k}\frac{\partial G}{\partial x_k}\right) f(G)\right]^{-1}. \tag{3.40}$$

It should be noted that $\langle R \rangle$ is constructed in such a way that (3.39) for the time-averaged flow is similar in form to the level-set form of the equations shown in (3.22) for the instantaneous flow.

Upon combining these three sets of terms, the time-averaged momentum equation for turbulent two-fluid flow is

$$\begin{aligned}\overline{\rho}\left[\frac{\partial \widehat{U}_i}{\partial t} + \widehat{U}_j\frac{\partial \widehat{U}_i}{\partial x_j}\right] = &-\frac{\partial \overline{P'}}{\partial x_i} - \frac{\partial \overline{\rho \widehat{u_i u_j}}}{\partial x_j} + \frac{\partial}{\partial x_j}\left[\overline{\mu}\left(\frac{\partial \widehat{U}_i}{\partial x_j} + \frac{\partial \widehat{U}_j}{\partial x_i}\right)\right] + \frac{\partial}{\partial x_j}\left[\overline{\mu}\left(\widehat{\frac{\partial u_i}{\partial x_j}} + \widehat{\frac{\partial u_j}{\partial x_i}}\right)\right] \\ &+ \frac{\partial}{\partial x_j}\langle \mu S_{ij} \rangle + \left[(\rho_1 - \rho_\circ)\, gz + \frac{\gamma}{\langle R \rangle}\right]\frac{\partial G}{\partial x_i} f(G).\end{aligned} \tag{3.41}$$

This equation, together with the continuity equation

$$\frac{\partial \overline{\rho}}{\partial t} + \frac{\partial}{\partial x_i}\left(\overline{\rho}\ \widehat{U}_i\right) = 0, \tag{3.42}$$

and the evolution equation for the mean free surface

$$\left(\frac{\partial G}{\partial t} + \widehat{U}_i \frac{\partial G}{\partial x_i}\right) f(G) - \frac{\overline{\rho}}{(\rho_\circ - \rho_1)} \frac{\partial \widehat{U}_i}{\partial x_i} = 0, \tag{3.43}$$

constitute a complete set of governing equations for the flow.

The resulting equations (3.41) to (3.43) have several desirable characteristics. In the limit of vanishing surface-elevation fluctuations, the mean fluid properties $\overline{\rho}$ and $\overline{\mu}$ become constant, the density-weighted averages reduce to simple time averages, and the second and third terms containing viscosity in (3.41) vanish. The p.d.f. $f(G)$ becomes a delta function indicating the position of the free surface, and so the G reduces to H and $\langle R \rangle$ reduces to R. Hence, the equations reduce to the conventional RANS equations of the level-set form. In the limit of laminar flow, they reduce to the level-set formulation of Chang *et al.* (1996). This is required for the formulation to be physically correct. In addition, the quantities which appear in the equations are measurable, and in some cases, are routinely measured, at present. For example, the velocity statistics measured by laser velocimeter in the liquid phase of an air–water flow (such as those shown above) are, in effect, density-weighted averages, since the measurements are made only when the liquid phase is present and the density of the air can be considered negligible relative to the density of the water. This allows experimental verification of any predictions made using the equations, and the use of experimental data in guiding the development of modelling approaches.

It should be noted that the set of equations (3.41) to (3.43) are mathematically exact, in the sense that no modelling has been introduced; however, they do not represent a closed system of equations. As is the case with the usual Reynolds-averaging process, additional unknowns are introduced owing to the loss of information. For the present set of equations, these additional unknowns are the Reynolds stresses $\widehat{u_i u_j}$, the fluctuating strain rate terms $\partial u_i / \partial x_j$, the viscous stress term $\langle \mu S_{ij} \rangle$, the effective mean surface curvature $1/\langle R \rangle$, and the p.d.f. of the surface elevation $f(G)$. For the unknowns beyond the Reynolds stresses, appropriate turbulence models must be developed to allow the set of equations to be closed. In addition, development of specific solution methodologies for the resulting closed system of equations may be required. While both of these are beyond the scope of the present study, the equations in the form presented above can be used in interpreting observed behaviour in free-surface turbulent flows, as will be shown in the next section.

4. High-Froude-number jet spreading

In this section, the above-developed equations are used to examine the origin of the surface current in high-Froude-number jet flows. For a turbulent jet issuing beneath a free surface, the jet initially evolves in a manner similar to a jet in an unbounded medium – a deep jet. Eventually, the jet begins to interact with the free surface. Once interaction with the free surface begins, it will be assumed that, except for a thin layer near the surface, the jet continues to behave as a deep jet. (That this is a reasonable assumption was demonstrated in Walker 1997.) In what follows, the form of the Reynolds-averaged Navier–Stokes equations governing the behaviour of the thin region near the free surface will be determined. The origin of the surface current for this flow will then be examined.

4.1. *Governing equations*

The governing equations derived in § 3 can be reduced under the assumption of the ideal free-surface condition, $\rho_1 = 0$. The time-averaged momentum equation (3.41) becomes

$$\overline{\rho}\widehat{U}_j\frac{\partial\widehat{U}_i}{\partial x_j} = -\frac{\partial\overline{P'}}{\partial x_i} - \frac{\partial\overline{\rho}\widehat{u_i u_j}}{\partial x_j} - \left[\rho_\circ g z - \frac{\gamma}{\langle R\rangle}\right]\frac{\partial G}{\partial x_i}f(G) + \frac{\partial}{\partial x_j}\left[\overline{\mu}\left(\frac{\partial\widehat{U}_i}{\partial x_j} + \frac{\partial\widehat{U}_j}{\partial x_i}\right)\right] + \frac{\partial}{\partial x_j}\left[\overline{\mu}\left(\widehat{\frac{\partial u_i}{\partial x_j}} + \widehat{\frac{\partial u_j}{\partial x_i}}\right)\right], \tag{4.1}$$

Equation (4.1) can be non-dimensionalized using the local characteristic scales of the jet, $U_\circ$ for the velocity scale and ℓ for the lengthscale. These length and velocity scales are representative of the local large-scale structures in the jet, i.e. the energy-containing scales. Non-dimensionalization yields, for the momentum equations under conditions of stationary flow,

$$\widehat{U}'_j\frac{\partial\widehat{U}'_i}{\partial x'_j} = -\frac{1}{F_\circ}\frac{\partial\overline{P'}'}{\partial x'_i} - \frac{1}{F_\circ}\frac{\partial F_\circ\widehat{u'_i u'_j}}{\partial x'_j} - \frac{1}{F_\circ}\left[\frac{z'}{Fr_l^2} - \frac{1}{We_l\langle R'\rangle}\right]\frac{\partial G}{\partial x'_i}f(G) + \frac{1}{Re_l}\frac{1}{F_\circ}\frac{\partial}{\partial x'_j}\left[F_\circ\left(\frac{\partial\widehat{U}'_i}{\partial x'_j} + \frac{\partial\widehat{U}'_j}{\partial x'_i}\right)\right] + \frac{1}{Re_l}\frac{1}{F_\circ}\frac{\partial}{\partial x'_j}\left[F_\circ\left(\widehat{\frac{\partial u'_i}{\partial x'_j}} + \widehat{\frac{\partial u'_j}{\partial x'_i}}\right)\right], \tag{4.2}$$

where $F_\circ = \overline{\rho}/\rho_\circ$, $Re_l = U_\circ\ell/\nu_\circ$ is the Reynolds number, $Fr_l = U_\circ/\sqrt{g\ell}$ is the Froude number, $We_l = \rho_\circ U_\circ^2\ell/\gamma$ is the Weber number, and all the variables are now non-dimensional (indicated by the primes). These definitions of Reynolds number and Froude number are strictly used for the order-of-magnitude analysis.

For a single lengthscale ℓ, a single velocity scale $U_\circ$, and a fixed set of fluid properties, only two independent dimensionless groups can be defined (i.e. the Weber number is set by specifying Reynolds number and Froude number). As a result

$$\frac{We_l}{Fr_l^2} = \frac{\rho_\circ\nu_\circ^{4/3}g^{1/3}}{\gamma}\left(\frac{Re_l}{Fr_l}\right)^{4/3} = 2.94\times10^{-4}\left(\frac{Re_l}{Fr_l}\right)^{4/3}, \tag{4.3}$$

for water at standard conditions. For the free-surface jet to be examined below, where the jet begins to interact with the free surface, the Reynolds number based on the local large-scale structure is 12 700 and the Froude number is about 2.8. This yields $We_l/Fr_l^2 \sim 20$ which indicates that, for this case, the effects of surface tension will be small relative to those of gravity. The high Reynolds number and the lack of no-slip boundaries together indicate that viscous effects will be negligible. Ignoring these effects, the reduced form for the momentum equations is

$$\overline{\rho}\widehat{U}_j\frac{\partial\widehat{U}_i}{\partial x_j} = -\frac{\partial\overline{P'}}{\partial x_i} - \frac{\partial\overline{\rho}\widehat{u_i u_j}}{\partial x_j} - \rho_\circ g z\frac{\partial G}{\partial x_i}f, \tag{4.4}$$

where the equations are now, again, in dimensional form.

It will be assumed that for the turbulent free-surface jet flows, the free surface will be a single-valued function of the horizontal coordinates x and y. Under this assumption, G will be defined as

$$G = \frac{(z-\overline{\eta})}{\eta'}, \tag{4.5}$$

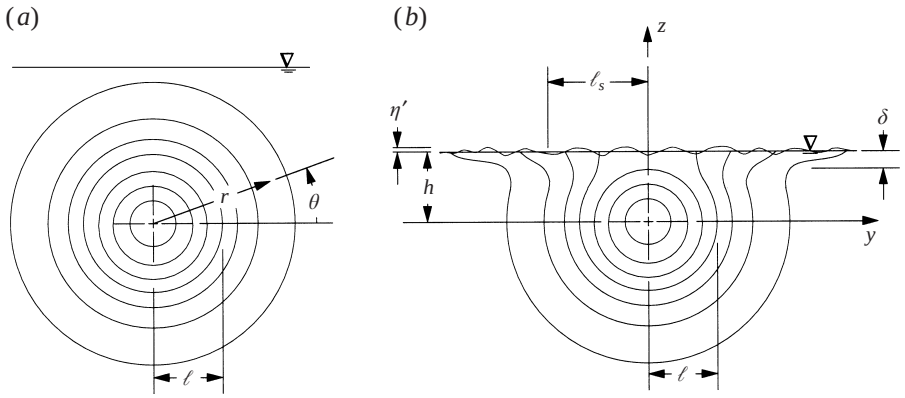

FIGURE 6. Schematic of streamwise velocity contours in a plane normal to the jet axis illustrating lengthscale definitions. (*a*) Streamwise velocity contours for a deep jet showing the (r, θ) coordinate system and the characteristic lengthscale ℓ. (*b*) Streamwise velocity contours for a free-surface jet (after Anthony & Willmarth 1992) showing the (y, z) coordinate system, the characteristic lateral lengthscale ℓ_s and vertical lengthscale δ and η' for the surface-current layer.

where, $\overline{\eta}$ is the mean free-surface position and η' is the r.m.s. of surface elevation. The level surfaces of G represent surfaces of constant probability for the free-surface location. The gradient of G is written as

$$\frac{\partial G}{\partial x_i} = -\frac{1}{\eta'}\left[\left(\frac{\partial \overline{\eta}}{\partial x} + G\frac{\partial \eta'}{\partial x}\right)\hat{\boldsymbol{i}} + \left(\frac{\partial \overline{\eta}}{\partial y} + G\frac{\partial \eta'}{\partial y}\right)\hat{\boldsymbol{j}} - \hat{\boldsymbol{k}}\right]. \tag{4.6}$$

4.2. *Order of magnitude analysis*

The following development will follow closely the analysis of Walker (1997). It was shown in that study that the evolution of the jet is unaffected by the free-surface except for a thin layer adjacent to the surface. Hence, outside the surface layer, the jet evolves as a deep jet. The key result from the deep jet analysis, as shown by Walker (1997), is

$$\frac{1}{\rho_\circ}\frac{\partial \overline{P'}}{\partial r} = -\frac{\partial \overline{u_r^2}}{\partial r}, \tag{4.7}$$

where r is the radial coordinate. In arriving at that result, a local turbulent velocity scale $u_\circ$, where $u_\circ^2 \sim U_\circ^2/10$, was introduced in addition to $U_\circ$ and ℓ, which are the maximum axial velocity and lateral lengthscale, respectively. Equation (4.7) relates the change in mean pressure to the transverse gradients in the $\overline{u_r^2}$ Reynolds stress. Integrating (4.7) yields

$$\frac{\overline{P'}}{\rho_\circ} + \overline{u_r^2} = \text{constant}. \tag{4.8}$$

It clearly shows that as the jet axis is approached from far away (where $\overline{P'}$ is constant), the mean pressure drops in proportion to the increase in $\overline{u_r^2}$. As a result, the minimum mean pressure will typically occur in the core of the jet where the turbulence level is greatest.

When the jet grows to the extent that it interacts with the free surface, the surface will begin to deform and a thin layer will form where the effects of the surface will be manifest. This layer grows laterally at a higher rate than the subsurface portion of the jet. The lateral lengthscale ℓ_s for the layer is larger than ℓ, the lateral scale of

the subsurface portion of the jet. A schematic of the resulting flow is shown in figure 6(*b*).

The following analysis will examine the region far enough downstream of the jet exit that h/x is small (where h is the depth of the jet axis beneath the free surface – see figure 6*b*), and the maximum axial velocity $U_\circ$ occurs near the free surface. In this region, the velocity scales $U_\circ$ and $u_\circ$, used in the deep-jet analysis, are also appropriate for the near-surface region. This behaviour occurs for $x/d > \sim 20$ (Walker *et al.* 1995). In this streamwise region, outside the near-surface layer, the jet will behave as a deep jet (Walker 1997).

For the near-surface region, vertical gradients could either be scaled using the surface-layer thickness δ, or the free-surface fluctuation level η'. However, the experimental data suggests η' is substantially smaller than δ and so δ will be used, except for terms which contain the surface fluctuation level explicitly. Using the appropriate lengthscales to non-dimensionalize the terms in the continuity equation indicates that the scale for the lateral mean velocity $\widehat{V}$ is $U_\circ \ell_s/x$, and the scale for the vertical mean velocity $\widehat{W}$ is $U_\circ \delta/x$. Since $\delta \ll x$ in this region, $\widehat{W} \ll \widehat{U}$. At this point the magnitude of ℓ_s is undetermined; however, it is expected to be smaller than x.

The above scaling can be applied to the momentum equations to identify the dominant terms in the near-surface region. Combining (4.4) and (4.6), the z-momentum equation, in Reynolds-averaged form, neglecting viscous and surface tension effects, is given by

$$\overline{\rho}\left[\widehat{U}\frac{\partial \widehat{W}}{\partial x} + \widehat{V}\frac{\partial \widehat{W}}{\partial y} + \widehat{W}\frac{\partial \widehat{W}}{\partial z}\right] = -\frac{\partial \overline{P'}}{\partial z} - \frac{\partial \overline{\rho}\widehat{uw}}{\partial x} - \frac{\partial \overline{\rho}\widehat{vw}}{\partial y} - \frac{\partial \overline{\rho}\widehat{w^2}}{\partial z} - \frac{1}{\eta'}\rho_\circ g z f, \tag{4.9}$$

$$\left(\frac{\delta}{x}\right) \quad \left(\frac{\delta}{x}\right) \quad \left(\frac{\delta}{x}\right) \quad \left(\frac{\Delta \overline{P'}}{\rho_\circ U_\circ^2}\frac{x}{\delta}\right)\left(R_{uw}\frac{u_\circ^2}{U_\circ^2}\right)\left(R_{vw}\frac{u_\circ^2}{U_\circ^2}\frac{x}{\ell_s}\right)\left(\frac{u_\circ^2}{U_\circ^2}\frac{x}{\delta}\right)\left(\frac{gx}{U_\circ^2}\right).$$

The second line of (4.9) shows the order of magnitude estimates for the terms, divided by $\rho_\circ U_\circ^2/x$, in a manner similar to that of Walker (1997). Note that δ is used as the vertical lengthscale for all terms except the last, for which η' is the proper vertical scale. The order estimate for the final term reflects that $zf/\eta' \sim O(1)$.

The first three terms in (4.9) are clearly negligible, since $\delta \ll x$. The magnitude of the pressure term is undetermined. The terms involving $\widehat{uw}$ and $\widehat{vw}$ will be negligible since $R_{uw} \ll 1$ and $R_{vw} \ll 1$ in the near-surface region (see e.g. Anthony & Willmarth 1992). The remaining three terms will be non-negligible for arbitrary-Froude-number flows. Retaining all the non-negligible terms in (4.9) yields

$$\frac{\partial \overline{P'}}{\partial z} = -\frac{\partial \overline{\rho}\widehat{w^2}}{\partial z} - \frac{1}{\eta'}\rho_\circ g z f. \tag{4.10}$$

This shows that for general, non-zero-Froude-number flows, surface disturbances contribute to local mean pressure in the region where the p.d.f. is non-zero. For zero-Froude-number flows, η' goes to zero and the second term on the right-hand side vanishes for the subsurface flow, but applies at the surface (it becomes part of the boundary condition). For that case, the pressure gradient in the vertical direction is determined by the gradient of the $\widehat{w^2}$ normal stress ($\widehat{w^2} = \overline{w^2}$ for zero-Froude-number flows), and $\Delta \overline{P'} \sim \rho_\circ u_\circ^2$, which is consistent with Walker (1997).

At a given streamwise position, (4.10) can be integrated to yield

$$\overline{P'}(y,z_\circ)=\overline{P'}_\infty(y)+\rho_\circ\widehat{w^2}_\infty(y)-\overline{\rho}(y,z_\circ)\widehat{w^2}(y,z_\circ)-\frac{\rho_\circ g}{\eta'}\int_{-\infty}^{z_\circ} fz\ \mathrm{d}z \tag{4.11}$$

for the pressure at $z=z_\circ$ in the near-surface layer. Here, the ∞ subscript represents the quantities evaluated at $z\to-\infty$, relative to the thin near-surface layer. The major conclusion obtained from the z–momentum equation is that the mean pressure $\overline{P'}$ in the near-surface layer is completely determined by the local level of $\widehat{w^2}$, the free-surface fluctuation level η' and the conditions at $z\to-\infty$, which, in this case, is the portion of the jet which still behaves as a deep jet. Outside the near-surface layer, where the flow behaves as a deep axisymmetric jet, (4.8) gives

$$\overline{P'}_\infty=-\rho_\circ\widehat{u^2_r}_\infty+\rho_\circ g\overline{\eta}\approx-\rho_\circ\widehat{w^2}_\infty+\rho_\circ g\overline{\eta}. \tag{4.12}$$

(The term $\rho_\circ g\overline{\eta}$ is added to account for mean surface elevation changes appropriately.) Substituting (4.12) into (4.11) yields

$$\overline{P'}(y,z_\circ)=-\overline{\rho}\widehat{w^2}(y,z_\circ)-\frac{\rho_\circ g}{\eta'}\int_{-\infty}^{z_\circ} fz\ \mathrm{d}z+\rho_\circ g\overline{\eta}. \tag{4.13}$$

This result shows that the pressure in the near-surface region can be written in terms of the local $\widehat{w^2}$, the surface fluctuation distribution and the mean surface elevation. If it is assumed that the surface elevation statistics are Gaussian (a reasonable assumption, given the results shown above in figure 5),

$$f=\frac{1}{\sqrt{2\pi}}\,\mathrm{e}^{-1/2G^2}, \tag{4.14}$$

and (4.13) becomes

$$\overline{P'}(y,z_\circ)=-\overline{\rho}\widehat{w^2}+\rho_\circ g\eta' f+\overline{\rho}g\overline{\eta}. \tag{4.15}$$

Attention is now turned to the y-momentum equation. It is anticipated that there will be a larger-magnitude outward $\widehat{V}$ in the near-surface layer (and as a result of continuity, a larger lateral lengthscale ℓ_s) than exists in the deep jet. The exact relationship of these near-surface scales to those in the deep jet, however, remains to be determined. The y–momentum equation is given by

$$\begin{gathered}\overline{\rho}\left[\widehat{U}\frac{\partial\widehat{V}}{\partial x}+\widehat{V}\frac{\partial\widehat{V}}{\partial y}+\widehat{W}\frac{\partial\widehat{V}}{\partial z}\right]=-\frac{\partial\overline{P'}}{\partial y}-\frac{\partial\overline{\rho}\widehat{uv}}{\partial x}-\frac{\partial\overline{\rho}\widehat{v^2}}{\partial y}-\frac{\partial\overline{\rho}\widehat{vw}}{\partial z}-\rho_\circ gzf\frac{\partial G}{\partial y},\\ \left(\frac{\ell_s}{x}\right)\quad\left(\frac{\ell_s}{x}\right)\quad\left(\frac{\ell_s}{x}\right)\qquad\left(\frac{u_\circ^2x}{U_\circ^2\ell_s}\right)\left(R_{uv}\frac{u_\circ^2}{U_\circ^2}\right)\left(\frac{u_\circ^2x}{U_\circ^2\ell_s}\right)\left(R_{vw}\frac{u_\circ^2x}{U_\circ^2\delta}\right)\end{gathered} \tag{4.16}$$

where the second line again contains the order-of-magnitude estimates normalized by $\rho_\circ U_\circ^2/x$. The last term in (4.16) is expanded as,

$$\begin{gathered}-\rho_\circ gzf\frac{\partial G}{\partial y}=\rho_\circ\frac{gzf}{\eta'}\frac{\partial\overline{\eta}}{\partial y}+\rho_\circ\frac{gzf}{\eta'}G\frac{\partial\eta'}{\partial y}\\ O\left(\frac{g\overline{\eta}}{U_\circ^2}\frac{x}{\ell_s}\right)\ O\left(\frac{g\eta'}{U_\circ^2}\frac{x}{\ell_s}\right).\end{gathered} \tag{4.17}$$

The term containing the $\widehat{vw}$ Reynolds stress will be negligible since v and w are uncorrelated ($R_{vw}\ll1$). Because $R_{uv}<1$ and $x/\ell_s>1$, the $\widehat{uv}$ term is of lower order than the lateral pressure and $\widehat{v^2}$ gradients, and can be neglected as well.

Walker (1997) showed that ℓ_s could not be so small that the advection terms were negligible (this would result in inconsistencies in the equations), and so the advection terms in (4.16) must be retained. The resulting form of the y-momentum equation is

$$\overline{\rho}\left[\widehat{U}\frac{\partial\widehat{V}}{\partial x}+\widehat{V}\frac{\partial\widehat{V}}{\partial y}+\widehat{W}\frac{\partial\widehat{V}}{\partial z}\right]=-\frac{\partial\overline{P'}}{\partial y}-\frac{\partial\overline{\rho}\,\widehat{v^2}}{\partial y}+\rho_\circ\frac{gzf}{\eta'}\frac{\partial\overline{\eta}}{\partial y}+\rho_\circ\frac{gzf}{\eta'}G\frac{\partial\eta'}{\partial y}. \quad (4.18)$$

Using (4.15) to eliminate the local pressure from (4.18) yields the y-direction momentum equation in the thin near-surface layer:

$$\overline{\rho}\left[\widehat{U}\frac{\partial\widehat{V}}{\partial x}+\widehat{V}\frac{\partial\widehat{V}}{\partial y}+\widehat{W}\frac{\partial\widehat{V}}{\partial z}\right]=-\frac{\partial}{\partial y}\left[\overline{\rho}\left(\widehat{v^2}-\widehat{w^2}\right)\right]-g\frac{\partial}{\partial y}(\overline{\rho}\,\overline{\eta})-\rho_\circ g\frac{\partial}{\partial y}(f\eta')$$
$$+\frac{\rho_\circ g}{\eta'}\left[\overline{\eta}f\frac{\partial\overline{\eta}}{\partial y}+\eta' fG\frac{\partial\overline{\eta}}{\partial y}+\overline{\eta}fG\frac{\partial\eta'}{\partial y}+\eta' fG^2\frac{\partial\eta'}{\partial y}\right]. \quad (4.19)$$

The first term on the right-hand side is turbulence anisotropy, and all the others are pressure force terms which are related to the surface fluctuation and mean free-surface gradients. This result, which is more general than that in Walker (1997), indicates that, for high-Froude-number flow with significant surface fluctuations and small anisotropy, the surface current will be driven mainly by the pressure forces associated with the surface fluctuations and mean free-surface slopes. On the other hand, for zero Froude number, all terms associated with the free surface vanish, and the surface current will be driven by the turbulence anisotropy, consistent with the results of Walker (1997). Note that this equation applies only in the thin surface layer above the region where the jet behaves like a deep jet.

Equation (4.19) can be integrated from $z=\overline{\eta}-\delta$ to $z=\infty$ to determine the total y-acceleration over the thin surface layer which drives the surface current. It is assumed that δ is somewhat larger than η' ($\delta>3\eta'$), and, therefore, the p.d.f. is zero at the lower limit of integration ($f|_{z=\overline{\eta}-\delta}=0$). In addition, it is assumed that $(\widehat{v^2}-\widehat{w^2})|_{z=\overline{\eta}-\delta}\ll(\widehat{v^2}-\widehat{w^2})|_{z=0}$. Integrating (4.19) then yields

$$\int_{\overline{\eta}-\delta}^{\infty}\overline{\rho}\left[\widehat{U}\frac{\partial\widehat{V}}{\partial x}+\widehat{V}\frac{\partial\widehat{V}}{\partial y}+\widehat{W}\frac{\partial\widehat{V}}{\partial z}\right]\mathrm{d}z=-\frac{\partial}{\partial y}\left[\int_{\overline{\eta}-\delta}^{\infty}\overline{\rho}(\widehat{v^2}-\widehat{w^2})\mathrm{d}z\right]-\rho_\circ g\delta\frac{\partial\overline{\eta}}{\partial y}-\frac{\rho_\circ g}{2}\frac{\partial\eta'^2}{\partial y}$$
$$\equiv-\frac{\partial}{\partial y}\langle\overline{\rho}(\widehat{v^2}-\widehat{w^2})\rangle-\rho_\circ g\delta\frac{\partial\overline{\eta}}{\partial y}-\frac{\rho_\circ g}{2}\frac{\partial\eta'^2}{\partial y}. \quad (4.20)$$

Hence, the average acceleration over the thin surface layer is related to the density-weighted integration of anisotropy, mean free-surface slope, and lateral gradient of surface fluctuation levels. It should be noted that only the first and last terms on the right-hand side of (4.20) are directly related to the turbulent velocity and free-surface fluctuations. The term involving $\overline{\eta}$ affects the entire water column, and therefore does not influence the near-surface region any more than it does the deep flow.

5. Comparison to experiment

The experimental data for the jet flows presented above can be used to verify that the foregoing analysis is consistent with observed behaviour. Since the analysis applies for $x/d>20$, the data presented above for $Fr=1.0$ and 8.0 at $x/d=32$ will be used. Figures 7(*a*) and 7(*b*) show $\widehat{U}$ normalized by $U_e d/x$ versus transverse position y/x at the free surface $z=2d$ and at the level of the jet axis $z=0$, respectively.

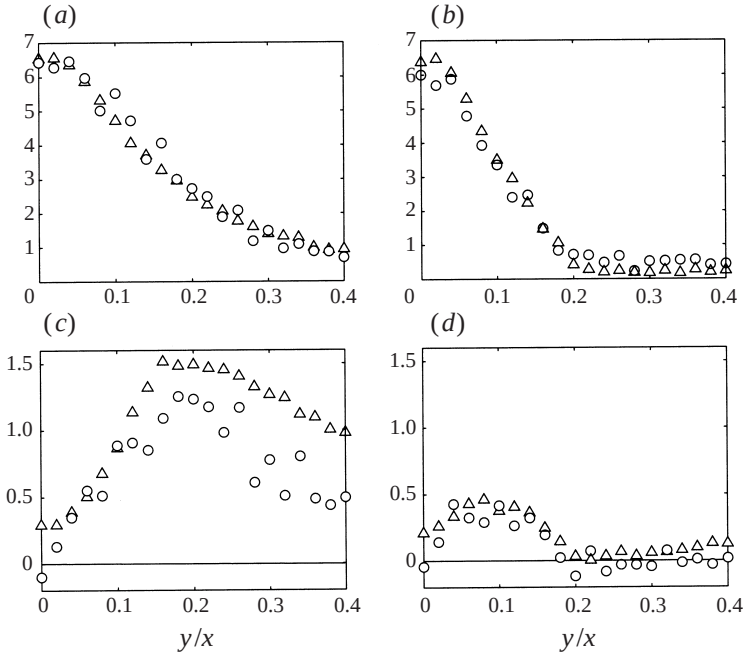

FIGURE 7. Profiles of mean streamwise velocity $\widehat{U}$ normalized by $U_e/(x/d)$ versus transverse coordinate y/x at $x/d = 32$, at (*a*) the free surface ($z = 2d$), and (*b*) the centreplane ($z = 0$); and mean transverse velocity $\widehat{V}$ normalized by $U_e/(x/d)$ versus transverse coordinate y/x at $x/d = 32$, at (*c*) the free surface ($z = 2d$), and (*d*) the centreplane ($z = 0$); △, $Fr = 8.0$; ○, $Fr = 1.0$.

The vertical symmetry plane of the jet corresponds to $y = 0$, on the left-hand edge of the figures. It can be seen that $\widehat{U}$ is similar for the two Froude numbers both at the free surface (figure 7*a*), and below the free surface (figure 7*b*). Figures 7(*c*) and 7(*d*) show similar plots of $\widehat{V}$ for $z = 2d$, and $z = 0$. Although there is more scatter in the data for $Fr = 1.0$ than for $Fr = 8.0$ (owing to the lower magnitude of the velocities in the $Fr = 1.0$ flow), some clear similarities, and clear differences, are observed. The subsurface flow is nearly identical for the two cases, as seen in figure 7(*d*). The maximum outward velocity at the free surface $z = 2d$, seen in figure 7(*c*), is roughly 3–4 times that in the deep portion of the jet at $z = 0$, shown in figure 7(*d*). In figure 7(*c*), it is clear that, for the high-Froude-number flow, the outward velocity is as much as twice as large as that for the low-Froude-number jet.

To verify (4.20) using the experimental data, the Reynolds-stress-difference (anisotropy) term $\langle\overline{\rho}(\widehat{v^2} - \widehat{w^2})\rangle$ was calculated by numerically integrating $\overline{\rho}(\widehat{v^2} - \widehat{w^2})$ over the near-surface region, from $z = d$ to $z = 2d$. This implies that $\delta \approx d$, which is consistent with the experimental data shown above for the Reynolds stress anisotropy and the transverse velocity. The measured Reynolds-stress difference at $z = d$ is about one-tenth that at $z = 2d$, as is the transverse velocity $\widehat{V}$, consistent with the assumption that these quantities become small at the lower edge of the near-surface layer. The result is plotted, along with the surface fluctuation term $\frac{1}{2}\rho_\circ g\eta'^2$ and the sum of the two terms, in figures 8(*a*) and 8(*b*) for the low- and high-Froude-number flows, respectively. The corresponding lateral gradients of these terms are plotted in figures 8(*c*) and 8(*d*), and $\partial\widehat{V}^2/\partial y$, indicative of the magnitude of the advection terms in (4.20), is plotted in 8(*e*) and 8(*f*), for the two flows.

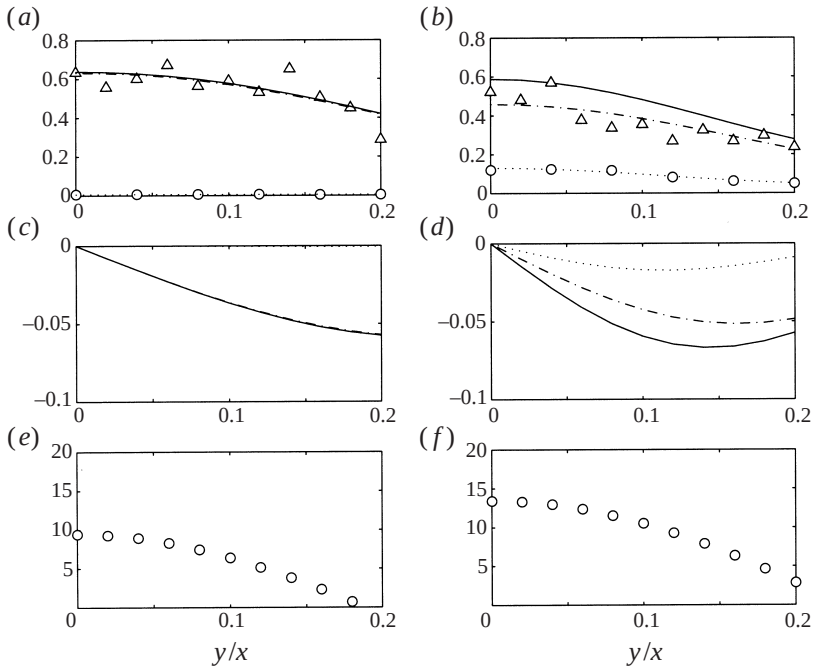

FIGURE 8. Profile of the terms in (4.20) versus transverse coordinate y/x at $x/d = 32$: (*a*) for $Fr = 1.0$: △ —·—, $\langle\overline{\rho}(\widehat{v^2} - \widehat{w^2})\rangle$; ○ · · ·, $\frac{1}{2}\rho_\circ g\eta'^2$; ————, sum of both terms; all terms normalized by $(U_e d/x)^2$; (*b*) for $Fr = 8.0$, symbols as in (*a*); (*c*) for $Fr = 1.0$: —·—, $\partial\langle\overline{\rho}(\widehat{v^2} - \widehat{w^2})\rangle/\partial y$; · · ·, $\partial(\frac{1}{2}\rho_\circ g\eta'^2)/\partial y$; ————, sum of both terms; normalized by $U_e^2 d/x^2$; (*d*) for $Fr = 8.0$, symbols as in (*c*); (*e*) for $Fr = 1.0$: $\partial\widehat{V}^2/\partial y$ at free surface $z = 2d$ normalized by $U_e^2 d/x^2$ (*f*) for $Fr = 8.0$, symbols as in (*e*).

Comparison of figures 8(*a*) and 8(*b*) shows that the surface fluctuation $\frac{1}{2}\rho_\circ g\eta'^2$ (the dotted line) is smaller in the low-Froude-number flow (figure 8*a*) than in high-Froude-number flow (figure 8*b*). Also, because of the larger anisotropy near the free surface in low-Froude-number flows, $\langle\overline{\rho}(\widehat{v^2} - \widehat{w^2})\rangle$ (the dash-dot line) is larger in figure 8(*a*) than in figure 8(*b*). The sum of the two terms (the solid line) in both high- and low-Froude-number cases have comparable magnitude. Equation (4.20) shows that the lateral acceleration associated with the surface current is related to lateral gradients of the Reynolds-stress difference $\langle\overline{\rho}(\widehat{v^2} - \widehat{w^2})\rangle$ and the surface fluctuation $\frac{1}{2}\rho_\circ g\eta'^2$; both gradients are shown in figures 8(*c*) and 8(*d*), along with their sum. In the low-Froude-number case (figure 8*c*), the lateral gradient of $\frac{1}{2}\rho_\circ g\eta'^2$ is negligible, compared with that of $\langle\overline{\rho}(\widehat{v^2} - \widehat{w^2})\rangle$. For high Froude number (figure 8*d*), the maximum lateral gradient of $\frac{1}{2}\rho_\circ g\eta'^2$ (the dotted line) is almost half the magnitude of the $\langle\overline{\rho}(\widehat{v^2} - \widehat{w^2})\rangle$ gradient (the dash-dot line). The sum of the lateral gradient of $\langle\overline{\rho}(\widehat{v^2} - \widehat{w^2})\rangle$ and $\frac{1}{2}\rho_\circ g\eta'^2$ (the solid line) is larger in the high-Froude-number flow. The plots of figure 8(*e*) and 8(*f*) show a larger outward acceleration $\partial\widehat{V}^2/\partial y$ in the $Fr = 8.0$ case, consistent with the data in figures 8(*c*) and 8(*d*).

These results indicate that the analysis of § 4 is consistent with observations for the region near $x/d = 32$, where the interaction of the free surface and the submerged turbulent jet is well established. For low-Froude-number flow, the surface fluctuations are negligible and the anisotropy alone drives the outward flow of the surface current.

For high-Froude-number flow, the weaker anisotropy is more than compensated for by the surface fluctuations, and results in a slightly larger outward acceleration.

6. Conclusions

This study has presented a formulation of the governing equations for Reynolds-averaged flow near a free surface. The resulting equations are written in terms of density-weighted averages and the p.d.f. of the free-surface elevation. The form of the continuity equation is identical to that of the conventional RANS equations, as is the form of the momentum equations, except for the addition of terms associated with the non-constant density, and terms which represent the effect of the forces acting instantaneously on the free surface. The surface forces, which are normally associated with the boundary conditions, are embedded in the field equations as apparent body forces. The region where these additional terms appear is defined by the p.d.f. of the surface elevation. An evolution equation derived from the averaged continuity equation describes the mean free-surface location.

The resulting equations have several desirable characteristics. In the limit of vanishing surface-elevation fluctuations, the equations reduce to the conventional RANS equations with separate boundary conditions. In the limit of laminar flow, they reduce to the level-set formulation of Chang *et al.* (1996). In addition, the quantities which appear in the equations are measurable and, in some cases, are routinely measured, at present. This will allow experimental verification of any predictions made using the equations, and the use of experimental data in guiding the development of modelling approaches.

The newly developed governing equations were used to examine the evolution of an initially axisymmetric jet interacting with a free surface. The purpose was to determine the origin of the surface current – the large outward velocity which exists in a thin layer adjacent to the surface. An appropriate form of the momentum equations for the near-surface region, valid for the region far-enough downstream of the jet exit that the maximum velocity occurs near the surface, was developed. It was shown that outward acceleration near the surface results from the lateral gradient in the near-surface anisotropy $\langle \overline{\rho}(\widehat{v^2} - \widehat{w^2}) \rangle$, and from the lateral gradient of the surface fluctuation level η'. This result is more general than that of Walker (1997), which included only the anisotropy, but applies strictly to zero-Froude-number flows. There is an additional contribution to lateral flow over the entire water column (not just near the free surface) from the lateral gradient of the mean surface elevation $\overline{\eta}$.

Comparison to available experimental data showed that the analysis is consistent with observed behaviour in free-surface jets for $x/d = 32$. For low-Froude-number flow, the surface fluctuations are negligible and the anisotropy alone appears to drive the surface current. For high-Froude-number flow, the weaker anisotropy is compensated for by the large free-surface fluctuation level and results in a slightly larger outward acceleration. The outward velocity at the surface for the high-Froude-number case is seen to be slightly larger, as would be expected.

This work was supported by the Office of Naval Research under Contract Nos. N00014-96-C-0038 and N00014-99-M-0082 at ERIM, and Grant Nos. N00014-94-1-1083 and N00014-97-1-0053 at the University of Michigan, all monitored by Dr E. P. Rood. The data presented in this study is part of a set collected by a number of undergraduate and graduate students over a three-year period, which represents more than two thousand hours of data acquisition. The diligence of B. Wildes, D.

Singer, G. Garwood, M. Eayre, M. Clark, B. Mehlhorn, and J. Samkowiak in that effort was, and is, greatly appreciated.

REFERENCES

Anthony, D. G. & Willmarth, W. W. 1992 Turbulence measurements in a round jet near a free surface. *J. Fluid Mech.* **243**, 699–720.

Aris, R. 1962 *Vectors, Tensors, and the Basic Equations of Fluid Mechanics*. Prentice-Hall.

Batchelor, G. K. 1967 *An Introduction to Fluid Dynamics*. Cambridge University Press.

Blaisdell, G. A. 1991 Numerical simulation of compressible homogeneous turbulence. PhD Dissertation. Stanford University.

Chang, Y. C., Hou, T. Y., Merriman, B. & Osher, S. 1996 A level-set formulation of Eulerian interface capturing methods for incompressible fluid flows. *J. Comput. Phys.* **124**, 449–464.

Davis, M. R. & Winarto, H. 1980 Jet diffusion from a circular nozzle above a solid wall. *J. Fluid Mech.* **101**, 201–221.

Duncan, J. 1993 Surface roughness in the wake of a steady breaking wave. *Proc. Third Intl Offshore and Polar Engng Conf. ISOPE*, pp. 39–44.

Hinze, J. O. 1975 *Turbulence*. McGraw-Hill, New York.

Launder, B. E. & Rodi, W. 1983 The turbulent wall jet – measurements and modeling. *Ann. Rev. Fluid Mech.* **15**, 429–459.

Logory, L. M., Hirsa, A. & Anthony, D. G. 1996 Interaction of wake turbulence with a free surface. *Phys. Fluids* **8**, 805–815.

Longo, J., Huang, H. P. & Stern, F. 1998 Solid/free-surface juncture boundary layer and wake. *Exps. Fluids* **25**, 283–297.

Mangiavacchi, N., Gundlapalli, R. & Akhavan, R. 1994 Dynamics of a turbulent jet interacting with a free surface. In *Free-Surface Turbulence* (ed. E. P. Rood & J. Katz). FED–181, ASME, pp. 69–82.

Naot, D. & Rodi, W. 1982 Calculation of secondary currents in channel flow. *J. Hydraul. Div. ASCE* **108**, 948–968.

Tahara, Y. & Stern, F. 1996 A large-domain approach for calculating ship boundary layers and wakes for nonzero Froude number. *J. Comput. Phys.* **127**, 398–411.

Walker, D. T. 1997 On the origin of the 'surface current' in turbulent free-surface flows. *J. Fluid Mech.* **339**, 275–285.

Walker, D. T., Chen, C.-Y. & Willmarth, W. W. 1995 Turbulent structure in free-surface jet flows. *J. Fluid Mech.* **291**, 223–261.

Walker, D. T. & Johnston, V. G. 1991 Observations of turbulence near the free surface in the wake of a model ship. In *Dynamics of Bubbles and Vortices Near a Free Surface* (ed. I. Sahin & G. Tryggvason). AMD-119, ASME.